

Automated Selection of Electron Neutrinos from the NuMI beam in the MicroBooNE Detector and Prospects for a Measurement of the Charged-Current Inclusive Cross Section

MICROBOONE-NOTE-1054-PUB

The MicroBooNE Collaboration

Email: MICROBOONE_INFO@fnal.gov

November 27, 2018

Abstract

We present a fully automated selection of NuMI beam produced electron neutrinos interacting in the MicroBooNE liquid argon time projection chamber operating at Fermilab. This analysis makes use of the Pandora reconstruction framework and subsequently a selection method developed specifically to select ν_e and $\bar{\nu}_e$ in data. The selection also utilizes one of liquid argon's signature capabilities, distinguishing electron-like and photon-like electromagnetic showers using dE/dx in data, as well as scintillation light-based timing. The studies presented here demonstrate a closure test of calculating the inclusive cross using Monte Carlo, where the input Monte Carlo cross section matches the extracted Monte Carlo cross section. From this we forecast the prospects of a future $\nu_e + \bar{\nu}_e$ cross section with MicroBooNE data.

Contents

1	Introduction	3
2	MicroBooNE Detector	3
3	NuMI Beam	4
3.1	Beamline Geometry	4
4	Data, Simulation and Event Reconstruction	6
4.1	Simulation	6
4.2	Event reconstruction	6
5	Electron Neutrino Event Selection	6
5.1	Signal Definition and Event Classification	7
5.2	Selection Cut Overview	7
5.3	Optical to TPC Information	8
5.4	Collection Plane Hits	9
5.5	dE/dx	10
6	Post-Selection	12
6.1	Selection Performance	12
6.2	Kinematics	13
7	Monte Carlo Cross Section Closure Test	15
7.1	NuMI Integrated Flux	15
7.2	Number of Target Nuclei	16
7.3	Events and Background	16
7.4	Efficiency	16
7.5	Estimation of Systematic Uncertainties	17
7.6	Monte Carlo Cross Section Calculation	17
8	Conclusion	17
A	Event Displays	18

1 Introduction

This note presents the MicroBooNE experiment's [1] automated selection of electron neutrino interactions in data coming from the Neutrino Main Injector (NuMI) beam at Fermilab towards a measurement of the inclusive electron neutrino charged-current cross section on argon. The signature of these events is at least a single electromagnetic (EM) shower in the final state - with or without associated tracks. We present the cuts used to obtain a sample of signal events in data and remove backgrounds coming mostly from cosmic ray interactions and photons originating from neutral-current interactions.

Electron-neutrino (ν_e) appearance is the “golden channel” in searches for the sterile neutrino in the SBN programme [2] and CP violation in the DUNE experiment[3]. Additionally, the energy of the NuMI flux at MicroBooNE extends up to several GeV (probing a large fraction of the proposed DUNE energy range) and has a higher intrinsic ν_e flux contribution than the Booster Neutrino Beam (BNB). These high-profile measurements will need precise position resolution and accurate particle identification offered by liquid argon time projection chamber detectors. In order to extract an oscillation probability from the number of observed events, the interaction cross section between electron neutrinos and argon needs to be known, as well as the relationship between true neutrino energy and observables such as lepton energy and angle,

There are few measurements of the ν_e charged-current (CC) cross section, e.g. those published by the MINER ν A [4] and T2K [5] experiments, however none use argon as a target. The MicroBooNE experiment has collected a significant amount of neutrino data from the NuMI beam and will be able to measure the ν_e cross section on argon for the first time. This note describes the first fully-automated inclusive ν_e selection on liquid argon using the Pandora software framework [6], and demonstrates the ability to isolate the ν_e signal from a large background of cosmogenic and neutrino backgrounds.

2 MicroBooNE Detector

MicroBooNE is one of three liquid argon time projection chambers (LArTPCs) in the SBN program and the first to begin data taking. Located at Fermilab on the Booster Neutrino Beam (BNB) and off-axis to NuMI beam [7], MicroBooNE's physics goal is to search for the excess of ν_e -like events reported by MiniBooNE [8], and determine whether it originates from neutrino interactions or other sources.

MicroBooNE is a liquid argon time projection chamber (LArTPC) detector, and therefore employs a combination of ionisation charge and scintillation light to measure the parameters of neutrino interactions. The ionisation charge is collected on three planes of read-out wires located on one side of the detector. Two of the planes detect the ionisation charge through induction, while the third collects the charge - these are known as the “induction” and “collection” wire planes respectively [9]. Behind the wire planes sit a plane of PMTs collecting optical information. These two complimentary techniques allow MicroBooNE to fully reconstruct neutrino interactions on argon in 3D (See Section 4.2). A detailed description of the MicroBooNE detector can be found in [1].

The convention used for defining the θ and ϕ angles in MicroBooNE is shown in Figure 1 and is based on the BNB direction. In this convention, θ is the polar angle and ϕ the azimuthal angle. The off-axis location of MicroBooNE with respect to the NuMI beam has the beam entering primarily at $\theta \approx 20$ degrees and $\phi \approx 8$ degrees.

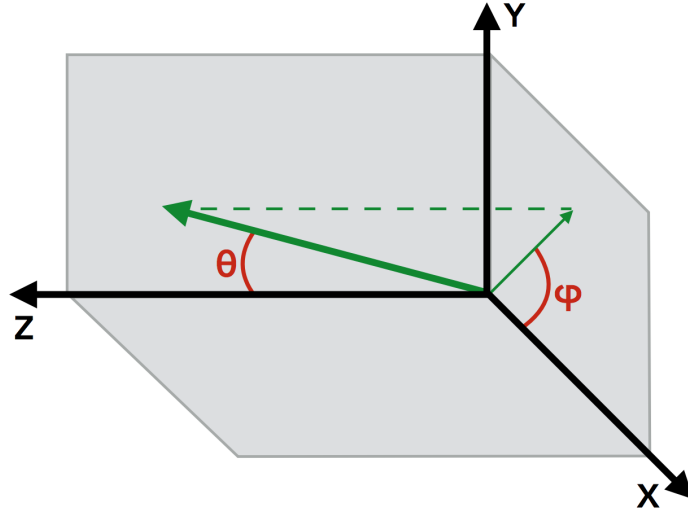


Figure 1: MicroBooNE coordinate system, where θ is the polar angle and ϕ the azimuthal angle [10]. The anode is located at $x = 0$ and the NuMI beam enters predominately at $\theta \approx 20$ degrees and $\phi \approx 8$ degrees.

3 NuMI Beam

MicroBooNE is approximately 8° off-axis to the NuMI beamline, where protons from the Main Injector Ring collide with a graphite target. The Main Injector is much larger in circumference than the Booster in order to contain the higher energy protons, which are accelerated up to 120 GeV. Due to the flexibility of the higher proton energy and configurations of the focusing horns, neutrinos with higher energy are produced on-average. More details on NuMI are found in [7].

3.1 Beamline Geometry

The geometry of the NuMI beam is designed for the long-baseline experiments MINOS and NO ν A, meaning the beam is shot at a 3° angle down into the Earth. Figure 2, top, shows the features of the NuMI beam such as the target hall, decay volume, and beam dump. Figure 2, bottom, then shows the aerial view of the NuMI beamline. Neutrinos are produced at the target with a direction of 20° upwards and 9° to the left reach MicroBooNE.

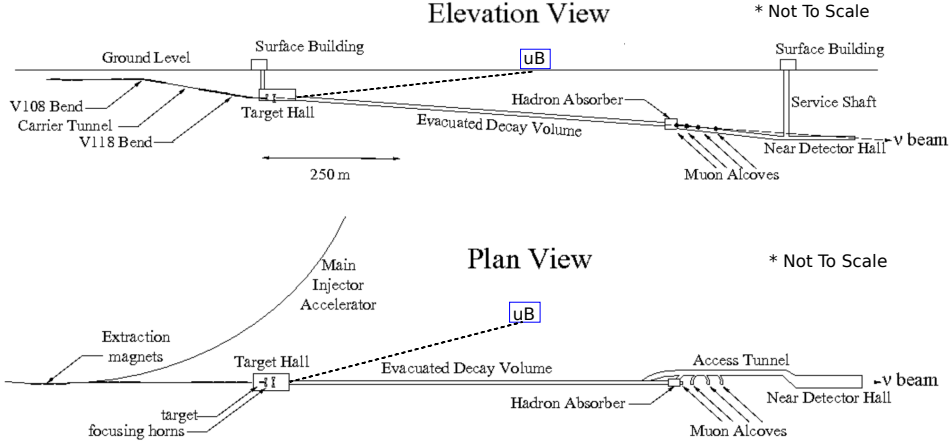


Figure 2: top: NuMI Beamline - the beam is angled downwards, such that neutrinos appear at the surface of the Earth for the NO ν A and MINOS far detectors; bottom: NuMI Beamline aerial view. Neutrinos produced at the target hall would need to exit approximately 8 degrees to the left to reach MicroBooNE [7].

Of the neutrinos reaching MicroBooNE, the majority are produced near the beam target. This is a convolution of the system's geometry and the rapid fall-off in intensity and energy as a function of the neutrino angle from the NuMI beamline. As a result fewer neutrinos originating from parent particle decays along the beam pipe reach MicroBooNE. The last and relatively small contribution of neutrinos comes from parent particles decaying in the beam dump.

Compared to the BNB, the NuMI flux at MicroBooNE has a higher intrinsic flux of ν_e and $\bar{\nu}_e$, primarily due to the kaon parent 3-body decays. Figure 3 shows the flux of the NuMI beam at MicroBooNE. Overall, the energy of the ν_e events is peaked at higher values than the BNB by approximately 200 MeV with a longer tail at higher energies, leading to a larger contribution from high-energy ν_e interactions. The very low energy ν_e events result from primarily decay-at-rest kaons, a sizeable fraction of which occur in the NuMI beam dump.

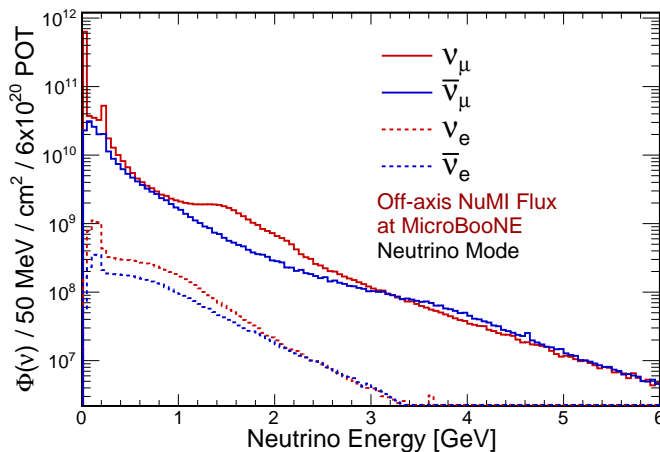


Figure 3: Off-Axis NuMI flux at MicroBooNE. Average neutrino energy is higher than BNB, however all neutrino flavours also have large contributions from very low energy decay-at-rest parents.

4 Data, Simulation and Event Reconstruction

The results shown here include data from the first run of MicroBooNE data-taking, in the period between February and June 2016, when the NuMI beam was in neutrino mode (forward horn current). The data acquired corresponds to 2.369×10^{20} proton on target (POT).

MicroBooNE has distinct trigger streams for both the On-Beam and Off-Beam (EXT) data. For On-Beam data, triggers are taken when accelerator signals indicate that protons are colliding with the NuMI target and producing neutrinos. For Off-Beam data a configurable pulser causes a trigger. Both trigger streams are independent of the BNB trigger streams allowing BNB and NuMI events to be easily distinguished from one another.

An online optical-based trigger in the data acquisition software checks for the presence of light in coincidence with the beam spill. If the light is below 9.5 photo-electrons (PE) the event is not saved. The off-beam data has the same trigger applied around a fake beam spill window the same size and the same time after the trigger is received - these samples of events are labelled BNB EXT and NuMI EXT. Further, the off-beam events are then prescaled so a random fraction of the events are saved. This is accounted for when normalising the two event distributions to the same exposure.

4.1 Simulation

Once the neutrinos reach MicroBooNE from the NuMI beam, their interactions are modelled using the GENIE MC simulation v2.12.2 [11]. GENIE simulates features of the interaction including: primary interaction with the nucleus, production of final-state particles in the nucleus, and transport and rescattering of final-state particles through the nucleus. Once the particles leave the nucleus, they are propagated through the detector using GEANT4. This includes the simulation of the electrons drifting to the wire planes and scintillation light propagated to the PMTs.

4.2 Event reconstruction

This analysis uses the Pandora [6] reconstruction framework, a series of algorithms working together to build representations of neutrino interactions. In this software package, hits are produced from the raw waveforms, and these hits are grouped together to form clusters. Clusters are matched between planes based on the hit times and known wire-crossing positions to form 3D objects. These objects are classified as either a track or a shower by Pandora, and many such objects are grouped together, intending to contain all neutrino interaction products.

The selection also makes use of MicroBooNE's optical system - a series of 32 PMTs. Interacting charged particles create scintillation light which is detected on the PMTs and is then reconstructed in both time and space. Such reconstructed optical signatures are called a "flash".

5 Electron Neutrino Event Selection

Pandora classifies each hierarchy as either an electron neutrino or a muon neutrino. This is done by identifying the object, or cluster, with the largest number of hits and assuming this is the lepton. If that object is a shower then it is classified as an electron neutrino by Pandora. This shower with the largest number of hits is referred to as the "leading shower".

5.1 Signal Definition and Event Classification

Signal events are defined as true ν_e or $\bar{\nu}_e$ charged-current interactions with their true vertex within the fiducial volume and a flash correlated with the neutrino beam. This signal definition is inclusive, meaning no requirement is made concerning the interaction type or final topology. This translates to a requirement of at least one reconstructed shower in the selection. The various classifications for signal and background events are listed below.

- **ν_e CC:** these are the signal events. The reconstructed object originates from a true ν_e or $\bar{\nu}_e$ CC which has its true interaction vertex inside the defined fiducial volume. This reconstructed object does not contain contributions from cosmic events (see **Mixed**).
- **ν_e CC Mixed:** mixed events refer to TPC objects which contain particles from a true ν_e or $\bar{\nu}_e$ CC interaction inside the fiducial volume, but also contain a particle with a cosmic origin. This most commonly occurs when cosmic events are located close to the neutrino interaction point, and Pandora wrongly creates an association between the two objects. These events are considered background events, as they have been incorrectly reconstructed.
- **ν_e CC OutFV:** while a fiducial volume cut is applied to the reconstructed neutrino vertex position, some true ν_e or $\bar{\nu}_e$ CC interactions are selected that have their true vertex outside of the fiducial volume. Aside from the reconstructed neutrino vertex position, these events have been correctly reconstructed. However because the vertex is outside the fiducial volume in truth, these events are categorized as backgrounds.
- **Cosmic:** specifically CORSIKA [12] generated cosmic interactions which have been overlain on top of the neutrino interactions. These events are cases where the neutrino event is concurrent with cosmic activity.
- **ν_μ CC:** these events are either pure or mixed ν_μ CC interactions.
- **NC:** the neutral current events are agnostic of the parent neutrino flavour, but are explicitly events which do not produce a true π^0 .
- **NC π^0 :** these neutral current events include only cases where at least one true π^0 is produced.
- **NC Mixed:** events classified as NC Mixed are any type of neutral current event (π^0 or not) which also have a cosmic particle object associated with the TPC Object.
- **Unmatched:** in a relatively small fraction of cases, the matching between a reconstructed object and a true object fails. In this case, the origin and parent information is unavailable and the event is classified as unmatched. This also encompasses cases where a particle object is created from a non-existing truth object. This could include cases where wire noise is reconstructed by Pandora.
- **In Time Cosmic:** while all other cases refer specifically to Monte Carlo classifications, the “In Time” events are coming exclusively from Off-Beam NuMI EXT data (see Section 4). These are background cosmic events which pass the neutrino selection cuts, but no neutrino is present in the event.

5.2 Selection Cut Overview

Identifying ν_e and $\bar{\nu}_e$ interactions is challenging, but Pandora is able to reconstruct approximately 70% of all NuMI $\nu_e/\bar{\nu}_e$ interactions inside the detector. However, due to the cosmic ray and beam-induced backgrounds, a series of selection cuts are needed to enhance the signal with respect to the background.

After all selection cuts, approximately 9% of true $\nu_e/\bar{\nu}_e$ interactions in the fiducial volume are selected, with a purity of 40%. To achieve this level of purity a number of selection cuts are applied and listed below for an overview. Cuts which form key steps in the analysis will be explained in greater detail below.

- **Reconstructed Shower in Fiducial Volume:** The reconstructed neutrino interaction is identified by Pandora’s algorithms to be ν_e -like. This means that a shower was reconstructed from the interaction and has a greater number of hits than any reconstructed tracks. The interaction also contains an optical flash correlated with the NuMI accelerator signal and a flash size of 50 PE. Lastly the reconstructed neutrino vertex must be inside the fiducial volume of 20 cm from all sides of the TPC.
- **Vertex to Flash Center:** Relationship between the reconstructed optical information and the reconstructed TPC information. The distance between the largest flash and the reconstructed neutrino vertex is used as a threshold - less than 80 cm forward, or less than 60 cm backwards. This is explained in more detail in Section 5.3.
- **Reconstruction Quality:** For event quality, the distance between the reconstructed neutrino vertex and corresponding tracks or showers are monitored. If the distance of any reconstructed track exceeds 4 cm from the reconstructed neutrino vertex, the event is removed. While for reconstructed showers, the requirement is made for at-least one shower being within 4 cm of the neutrino vertex.
- **Leading Shower Hit Threshold:** A minimum threshold is set for the leading shower’s wire plane activity. This takes two forms, first a minimum of 200 hits across all three wire planes. Second, specifically a minimum number of hits on the collection plane (Y-Plane) with a threshold of 80 hits. See Section 5.4 for more details.
- **Shower Opening Angle:** The opening angle is a feature of the reconstructed shower’s conical nature. Based on the characteristics of electromagnetic showers, a range between 2° and 15° controls for incorrectly or poorly reconstructed showers.
- **dE/dx:** The median dE/dx at the start of the shower is calculated. This is required to be in the range 1.4 MeV/cm to 3 MeV/cm to isolate the electron-like peak from photon-like backgrounds. See Section 5.5 for more details.
- **Shower Consistency:** A number of small cuts aimed at removing tracks which were reconstructed as showers, originating primarily from cosmic interactions. These involve checking properties such as the number of hits per unit length and the ratio of the shower to track lengths.
- **Track Containment:** The track containment cut requires that all tracks associated to a neutrino interaction have their reconstructed start and end points within the fiducial volume.

5.3 Optical to TPC Information

Cosmic-induced objects are the most common background, and it has been found that attempting to relate the optical information to the TPC information is an effective method for removing obvious cosmic events. This is done from a very simple relation which calculates the distance from the reconstructed optical centre with the most photo-electrons produced to the reconstructed TPC interaction vertex (this is calculated in plane of the PMTs). An asymmetric threshold is applied based on the relative relationships of the optical flash and the reconstructed vertex. When the flash position is more downstream than the vertex the threshold is placed at 80 cm, but when reversed is only 60 cm. Figure 4 shows how, in

general, signal events are within the cut threshold regions, while background events are removed. With this selection cut, the purity of the selection reaches 4%.

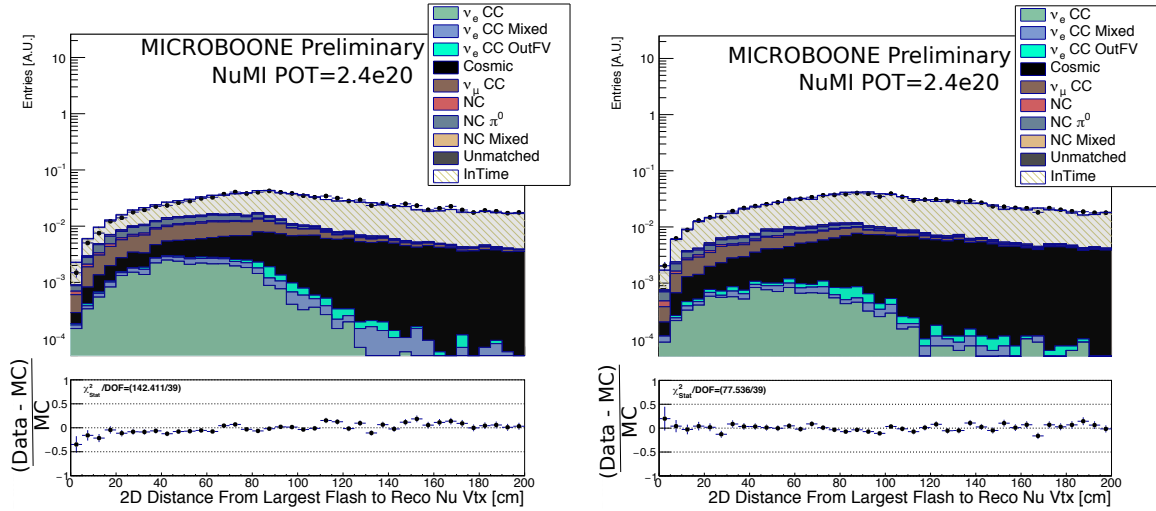


Figure 4: (Area Normalised) (Left) Flash is downstream w.r.t the reconstructed neutrino vertex. The signal events, along with other beam-induced events are clearly enhanced compared to the cosmic-induced. The threshold is placed at 80 cm. (Right) Flash is upstream w.r.t the reconstructed neutrino vertex. This case contains a much higher percentage of cosmics, therefore motivating the asymmetric application of threshold values. This threshold is placed at 60 cm.

5.4 Collection Plane Hits

Following on from selections cuts designed to improve the quality of the events selected, a cut on the number of hits for the leading shower is aimed at removing poorly reconstructed showers. One challenge for the current iteration of the reconstruction techniques used, is the mis-reconstruction of tracks as showers. The most common cases of this are often muon-like tracks that are short, change direction quickly, or pass through regions of the detector with poor sensitivity. This ultimately can result in small showers being reconstructed from track-like objects. A requirement that the leading shower has a minimum number of hits on the collection plane helps reduce these events, as seen in Figure 5, where a threshold of 80 hits is used. Showers with few hits on the collection plane can make calculating the dE/dx value difficult, making the collection plane hits cut also worth-while later in the selection chain. More details about the dE/dx implementation are described in Section 5.5.

Cutting on the leading shower hits on the collection plane leaves approximately 21% efficiency and 19.1% purity. By this stage the number of signal events is as large as the number of selected beam-induced backgrounds, however cosmic-induced backgrounds are roughly twice that of signal events.

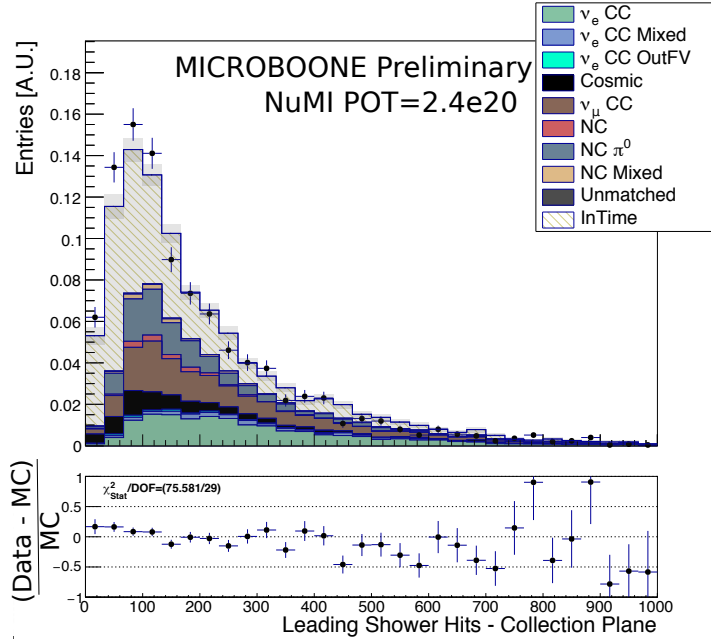


Figure 5: (Area Normalised) Number of hits for the leading shower on the collection plane. Background spectrum is clearly peaked below 80 hits, while most signal leading showers are at higher values.

5.5 dE/dx

One of the most powerful aspects of using LAr as a detector material is that MicroBooNE's whole volume is an active calorimeter. This means that the energy loss of particles can be observed cleanly along its trajectory which enables use of the energy-loss per unit length (dE/dx) to perform particle ID. This technique is critical for discerning showers induced by photon pair-production from the desired electron-induced showers and has been demonstrated in the ArgoNeuT detector [13]. The method for calculating the dQ/dx for shower is outlined below. We apply a 5% scaling to the data dE/dx values as a calibration in order to achieve agreement in the MIP region of this distribution. This is within the uncertainty on the estimated conversion factor from dQ/dx to dE/dx .

The dE/dx is calculated by constructing a $1 \times 4 \text{ cm}^2$ box around the reconstructed shower's start point, pointing in the reconstructed shower direction. Charge depositions on the collection plane are then sampled, where the collection plane has considerably higher signal-to-noise compared to the induction planes. ArgoNeuT found that using the median rather than the arithmetic mean produced more consistent results which were less sensitive to outlying hits depositing large amounts of charge [13]. We follow this approach here. Figure 6 shows a very rough schematic of this technique.

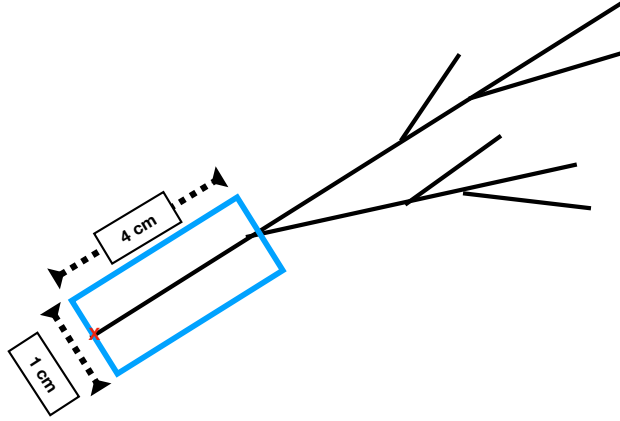


Figure 6: Rough schematic of the method used to calculate dQ/dx for reconstructed shower objects. The black lines represent a shower in the TPC. The blue box is the region sampled for calculating the dQ/dx and the red x shows the reconstructed shower vertex.

The dE/dx for the leading shower is shown in Figure 7. As expected, the signal distribution peaks in the 2 MeV/cm region. Large fractions of background lie to both sides of this peak, with cosmic interactions located primarily below 2 MeV/cm and an enrichment of π^0 events around 4 MeV/cm. The location of the π^0 peak is also in the expected region (reconstruction of 2 MIPs). However showers substantially below 2 MeV/cm result from limitations of MicroBooNE's current reconstruction techniques. The dE/dx can only be reliably calculated using information from the collection plane, meaning showers which are mostly parallel to the wire plane have little resolution with regards to their charge deposition. This limitation is well understood and can be corrected for by using dE/dx information from the two induction wire planes.

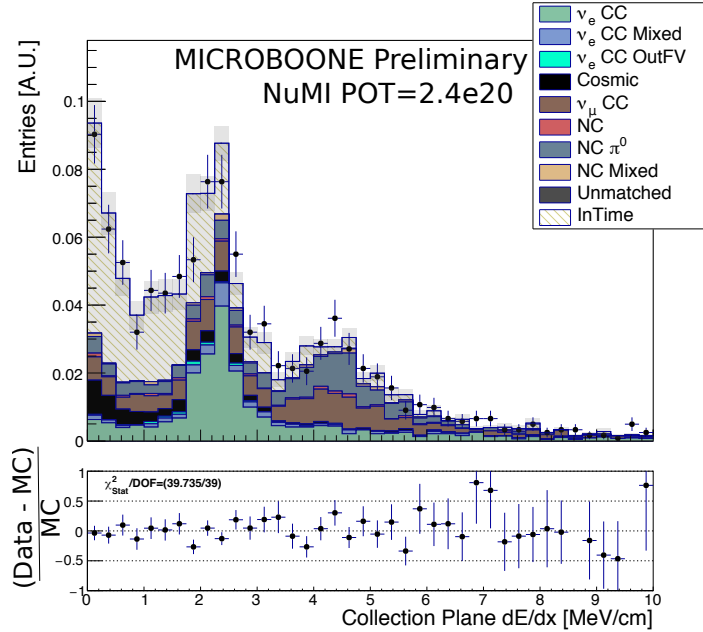


Figure 7: (Area Normalised) dE/dx distribution following the opening angle selection cut (immediately before the dE/dx cut is applied). Signal events are peaked at 2 MeV/cm and beam-induced backgrounds mostly peaked around 4 MeV/cm. Large amount of backgrounds are between 0 and 2 MeV/cm.

To isolate the signal peak, a cut between 1.4 MeV/cm and 3 MeV/cm is made, resulting in a drop of the selection efficiency to 11% and a large increase of the purity up to 30%. The strength of the dE/dx cut is emphasised by the fact that not only background π^0 events were removed, but also many mis-reconstructed track-like background events. This is a demonstration of MicroBooNE’s ability to differentiate between photon-like and electron-like showers.

6 Post-Selection

6.1 Selection Performance

After application of the secondary shower vertex, hits-per-length and track shower length ratio cuts which help ensure that the selected showers are actually “shower-like”, then the final cut requiring reconstructed track start and end points are within the fiducial volume is made. Figure 8 shows the selection efficiency as a function of the true electron energy and how it evolves after the application of various selection cuts. A summary of the selection cuts are found in Section 5.2, where the cut on the shower opening angle has been merged into the dE/dx cut for Figures 8 and 9. The shower consistency cuts have also been merged with the track containment cut to improve readability.

One of the obvious features in Figure 8 is the performance at very low electron energies, which noticeably suffers due to the difficulty in reconstructing such showers. Once the electron shower is successfully reconstructed, the decrease in performance due to selection cuts is relatively uniform. We expect that with improved reconstruction techniques, which are already in development, that more ν_e and $\bar{\nu}_e$ events will be recovered for further selections.

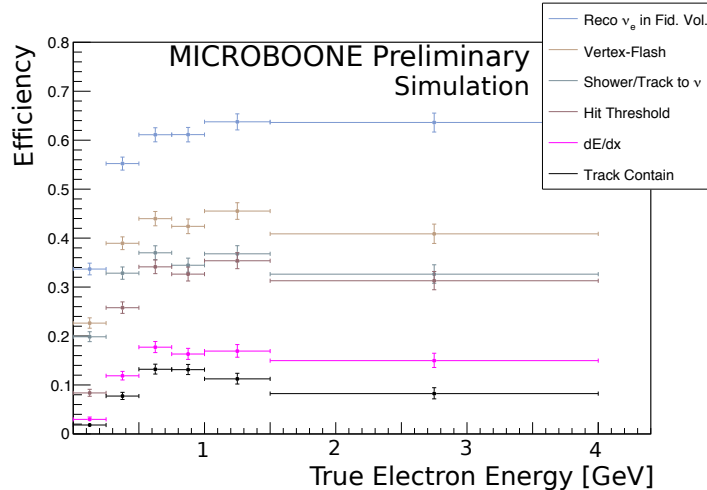


Figure 8: Efficiency overlay for the true electron energy coming from a true ν_e or $\bar{\nu}_e$ interaction. All selection cuts are shown, including the ability for Pandora to reconstruct the ν_e or $\bar{\nu}_e$.

The evolution of the total efficiency and purity can be seen in Figure 9, which shows the selection performance as a function of the individual cuts. The efficiency (green) decreases steadily as more cuts are applied down to approximately 9%. While the total purity (blue) gradually increases up to 40%, with perfect removal of cosmic events with no beam-induced signals, the beam only purity (purple) has a final value of 65%. With improvements to flash-matching and use of the Cosmic Ray Tagger (CRT) in future data-sets, we expect a significant reduction in selected cosmic events.

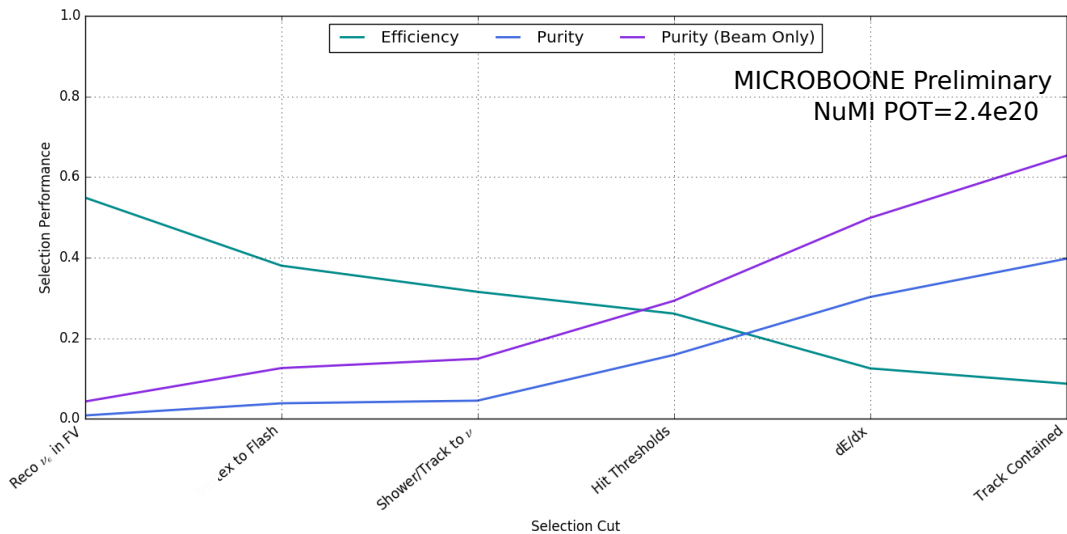


Figure 9: Summary of the selection performance, including efficiency, purity, and purity with no Off-Beam backgrounds. The Purity (Beam Only) case considers any beam-induced backgrounds, in addition to cosmic events crossing the neutrino interactions. Also note that the efficiency does not start at 100%, as approximately 25% of the true $\nu_e/\bar{\nu}_e$ cannot be reconstructed due to acceptance effects.

6.2 Kinematics

In this section we present sample area normalised distributions following the application of all selection cuts. These distributions give confidence that the analysis is selecting signal events in data, as well as

some information regarding the lepton kinematics.

For the NuMI beam in MicroBooNE, the off-axis nature gives rise to the ϕ distribution seen in Figure 10. Both the θ and ϕ distributions are shown in the MicroBooNE coordinate system shown above. The neutrinos coming directly from the target (as opposed to those from the beam dump, for example) enter MicroBooNE at a ϕ of approximately 25° . Around this direction, the signal is greatly enhanced compared to the background, while at larger values of ϕ the contamination from cosmics is much higher. This is because cosmic showers are often reconstructed as being either upward ($\phi = 90$) or downward ($\phi = -90$) going.

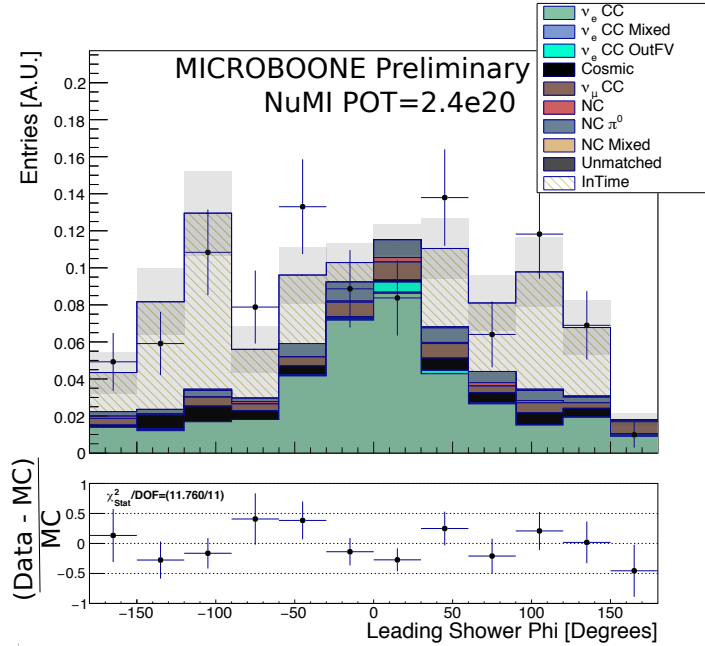


Figure 10: (Area normalised, MicroBooNE Coordinates) Leading shower ϕ for events which pass all selection cuts. The ϕ distribution is peaked for signal events at an angle consistent with the off-axis prediction of NuMI.

As mentioned in Section 5.5, due to the angle of the collection wire plane, events with a direction close to $\theta = 90^\circ$ are difficult to select. This behaviour is present in Figure 11. The vast majority of events are forward going ($< 90^\circ$). A small number of events are also backward going, but is primarily populated by cosmic events. Keeping this region of phase-space has two purposes - first this avoids making potentially model-dependent cuts on the shower angle. And second, the backwards region's agreement gives us confidence that the data and cosmic background match. The peak in the signal distribution is close to 40 degrees, rather than 0. This is because the NuMI target is several metres underground, causing all ν_e interactions to be upward going.

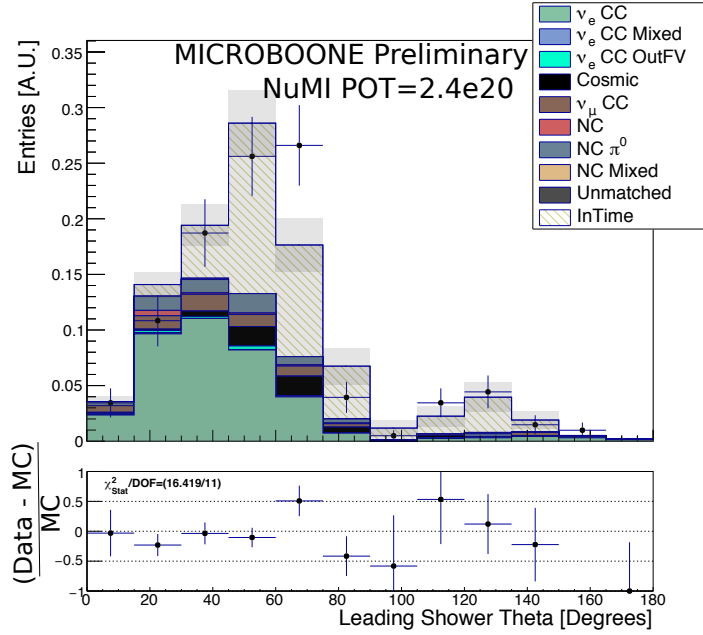


Figure 11: (Area normalised, MicroBooNE Coordinates) Leading shower θ for events which pass all selection cuts. The θ distribution is peaked in roughly the region expected based on the NuMI off-axis prediction. Forward-going showers appear favoured over backwards-going showers.

7 Monte Carlo Cross Section Closure Test

This section presents the method used to calculate the flux integrated Monte Carlo $\nu_e + \bar{\nu}_e$ CC cross section on argon. This calculation uses Monte Carlo events, but hopes to demonstrate the method and expected sensitivity of a future cross section measurement using data. For exclusively a flux-integrated cross section the calculation is relatively simple. Using the Equation 1, one can calculate the cross section σ :

$$\sigma = \frac{N - B}{\epsilon \times N_{Target} \times \Phi_{\nu_e + \bar{\nu}_e}} \quad (1)$$

where N is the total number of selected events, B the number of selected background events, ϵ the signal selection efficiency, N_{Target} the number of target nucleons and $\Phi_{\nu_e + \bar{\nu}_e}$ the integrated NuMI $\nu_e + \bar{\nu}_e$ POT-scaled flux.

7.1 NuMI Integrated Flux

Measured in the data is a combination of the $\nu_e + \bar{\nu}_e$ flux, but in Monte Carlo one can begin from the two separate fluxes. To determine the flux per POT, the NuMI flux prediction at MicroBooNE is used in Equation 2 and integrated over the energy range:

$$\phi = \int_{E_{Low}}^{E_{High}} \phi_E dE \quad (2)$$

where ϕ_E is the flux at a given energy. The number of ν_e or $\bar{\nu}_e$ per unit POT per cm^2 is:

$$\phi_{\nu_e} = 1.53 \times 10^{-11} \text{ cm}^{-2} \text{ POT}^{-1}$$

$$\phi_{\bar{\nu}_e} = 7.77 \times 10^{-12} \text{ cm}^{-2} \text{ POT}^{-1}$$

From here the Monte Carlo POT is applied (1.82×10^{21}) and the flux values used in the cross section calculations are calculated:

$$\Phi_{\nu_e} = 2.78 \times 10^{10} \text{ cm}^{-2}$$

$$\Phi_{\bar{\nu}_e} = 1.41 \times 10^{10} \text{ cm}^{-2}$$

7.2 Number of Target Nuclei

Calculating the number of nuclei is performed using a standard method. We can calculate N_{Target} using:

$$N_{Target} = \frac{\rho_{Ar} \times V \times N_A \times N_{Nucleons}}{m_{mol}} \quad (3)$$

where ρ_{Ar} is the density of liquid argon, V the fiducial volume, N_A Avagadro's Number, $N_{Nucleons}$ the number of nucleons per argon nucleus and m_{mol} the number of grams per mole of argon.

Parameter	Value
ρ_{Ar}	1.3954 g/cm ³
V	4.1622×10^7 cm ³
N_A	6.022×10^{23} molecule/mol
$N_{Nucleons}$	40.0
m_{mol}	39.95 g/mol

Table 1: Parameter list used to calculate the number of target nucleons in Monte Carlo.

Using these values and applying the formula above $N_{Target_{MC}}$ is calculated: 3.5019×10^{31} .

7.3 Events and Background

The values for N and B in the cross section formula are returned directly by the selection performance. For calculating an MC cross section N and B are known precisely. There are two parts to B :

$$B = B_{MC} + B_{EXT}$$

where B_{MC} are all Monte Carlo backgrounds and B_{EXT} are data-driven Off-Beam backgrounds. B_{MC} includes not only ν_μ CC interactions selected, but also the CORSIKA overlay cosmic events [12]. For Monte Carlo N is effectively $N = S + B$, where S is the number of Monte Carlo true signal events. Table 2 shows the relevant parameters for the Monte Carlo.

	S	B_{MC}	B_{EXT}	N
MC	628	352	610	1590

Table 2: Breakdown of number of signal and background events in Monte Carlo according to 1.82×10^{21} POT.

While the cross section is calculated using only Monte Carlo events, we take the statistical uncertainty derived from the number of selected data events, giving a value of 14% (stat).

7.4 Efficiency

The efficiency is a purely MC based value, calculated from the number of true selected events compared to the true signal events available in the sample. The result is $8.84\% \pm 0.09\%$, where the uncertainty is

derived from the Monte Carlo statistics.

7.5 Estimation of Systematic Uncertainties

Proper and careful treatment of the systematic uncertainties relevant to this analysis are still being considered, and therefore values quoted here are conservatively estimated. The primary source of these errors are in-line with other MicroBooNE analyses released around this time, including uncertainties from modeling in GENIE, detector-driven uncertainties, and flux uncertainties. Studies up to this point conservatively expect systematic uncertainties of 30%, with the NuMI flux uncertainty being the largest contribution.

7.6 Monte Carlo Cross Section Calculation

With all of the component values available, the Monte Carlo flux integrated cross section is calculated with all values shown in cm^2 for $\nu_e + \bar{\nu}_e$:

$$\sigma_{MC} (\nu_e + \bar{\nu}_e) = 4.83 \pm 0.69(\text{stat}) \pm 1.20(\text{sys}) \times 10^{-39} \text{cm}^2$$

where $\Phi_{\nu_e} + \Phi_{\bar{\nu}_e}$ is the integrated flux and the total number of signal events is $\nu_e + \bar{\nu}_e$ derived from the Monte Carlo.

A summary plot of the MC extracted cross section, along with the NuMI flux at MicroBooNE and the GENIE cross section splines is shown in Figure 12. The Monte Carlo band uses errors derived from the data measurement. For the y axis, this uses the 14% statistical uncertainty and then assumes an overall systematic uncertainty of 30%. These values were added in quadrature.

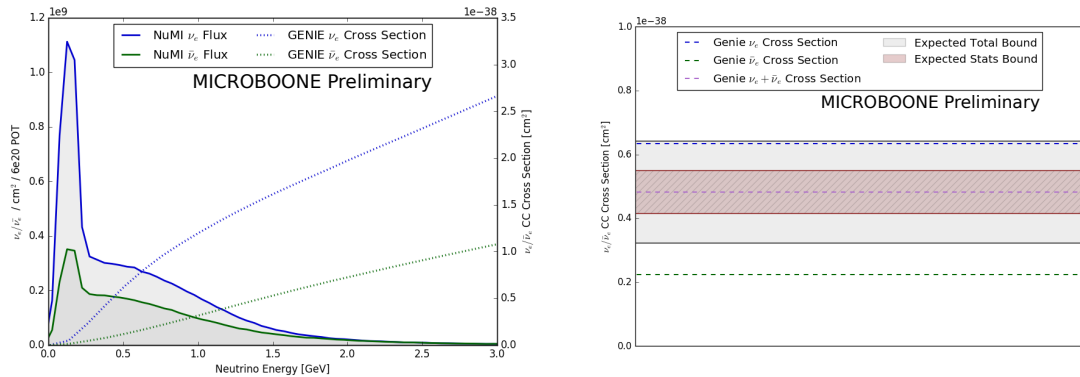


Figure 12: Monte Carlo extracted integrated cross section with expected data uncertainties. Blue lines correspond to ν_e and green to $\bar{\nu}_e$ and purple the flux average of the two. No data is shown, however the y-axis error bars are derived from the statistical uncertainty and a flat 30% systematic uncertainty is estimated to provide a realistic representation of the expected cross section.

8 Conclusion

This note demonstrates the application of one of liquid argon's most powerful techniques, calorimetric measurement of ionisation dE/dx of showers to separate electron-like and photon-like showers in data. Furthermore, the MC-based closure test demonstrates consistency of the analysis technique, whereby the extracted MC cross section value matches the input MC central value. We estimate that this analysis will be sensitive to the $\nu_e + \bar{\nu}_e$ CC inclusive cross section at the level of 14% (stat) + 30% (sys) uncertainty. Lastly we demonstrate MicroBooNE's ability to select and reconstruct ν_e and $\bar{\nu}_e$ events in data as a

proof of technique for extracting the inclusive NuMI flux-weighted $\nu_e + \bar{\nu}_e$ charged current cross section using data in the near future. This selection has been used to isolate approximately 100 signal events in data, making this the largest sample of ν_e events in Argon to-date.

A Event Displays

This appendix presents several event displays for NuMI On-Beam data events which have passed the event selection explained above.

Figure 13 demonstrates the selection's ability to find $\nu_e/\bar{\nu}_e$ candidate events in data, which mirror an expected topology of a single track and single shower interaction. The color scale shows different levels of charge deposition which can be calorimetrically reconstructed for both track-like and shower-like objects.

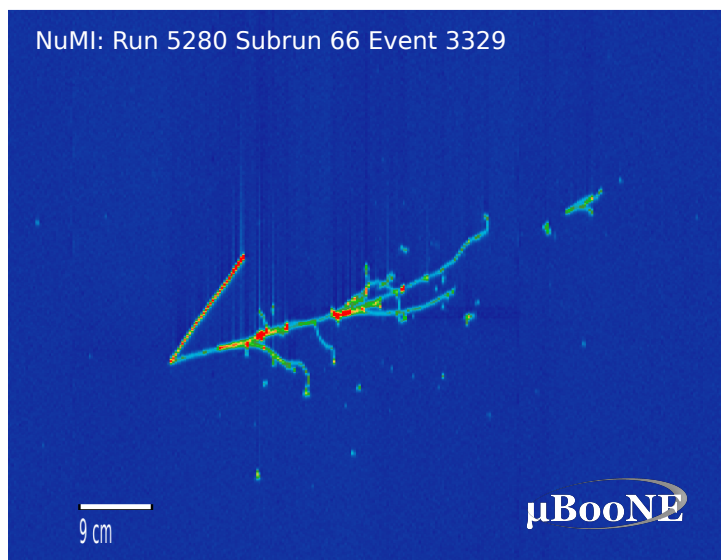


Figure 13: Single track, single shower interaction from the NuMI beam.

Figure 14 shows a 2.2 GeV shower with a length up to 1.5 meters, that is nicely resolved in the detector. This is within the expected energy range for events being measured by DUNE.

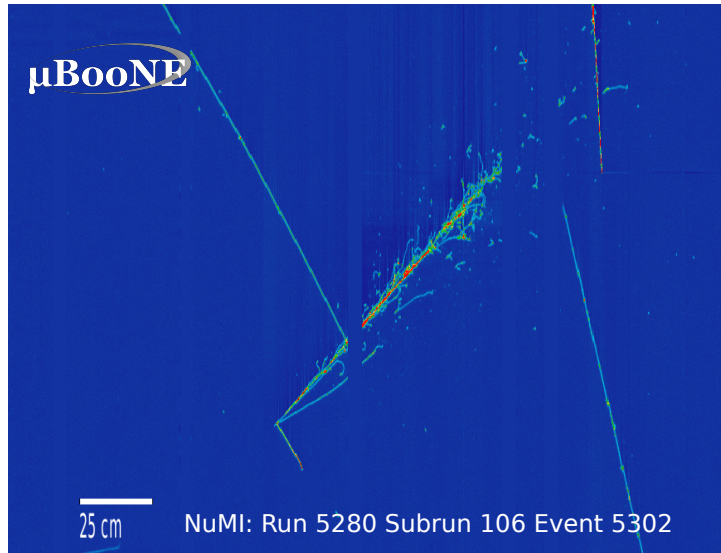


Figure 14: The large shower is successfully reconstructed as a single shower, despite a gap in sensitive wires. Both tracks emerging from the vertex are also reconstructed.

Figure 15 shows the same event across all three of MicroBooNE's wire planes. These three displays exemplify the benefits of redundancy in using three wires planes to reconstruct TPC objects. In the collection plane (Plane 2), the interaction vertex is not detected due to unresponsive wires, but being clearly visible on the other two wire planes. In the second induction plane (Plane 1), a number of cosmic tracks are crossing close to the event, but are successfully decoupled from the neutrino event by the reconstruction, as when projected into 3D space, the events are no longer overlapping. These displays demonstrate the power of having three wires planes available for use in analyses.

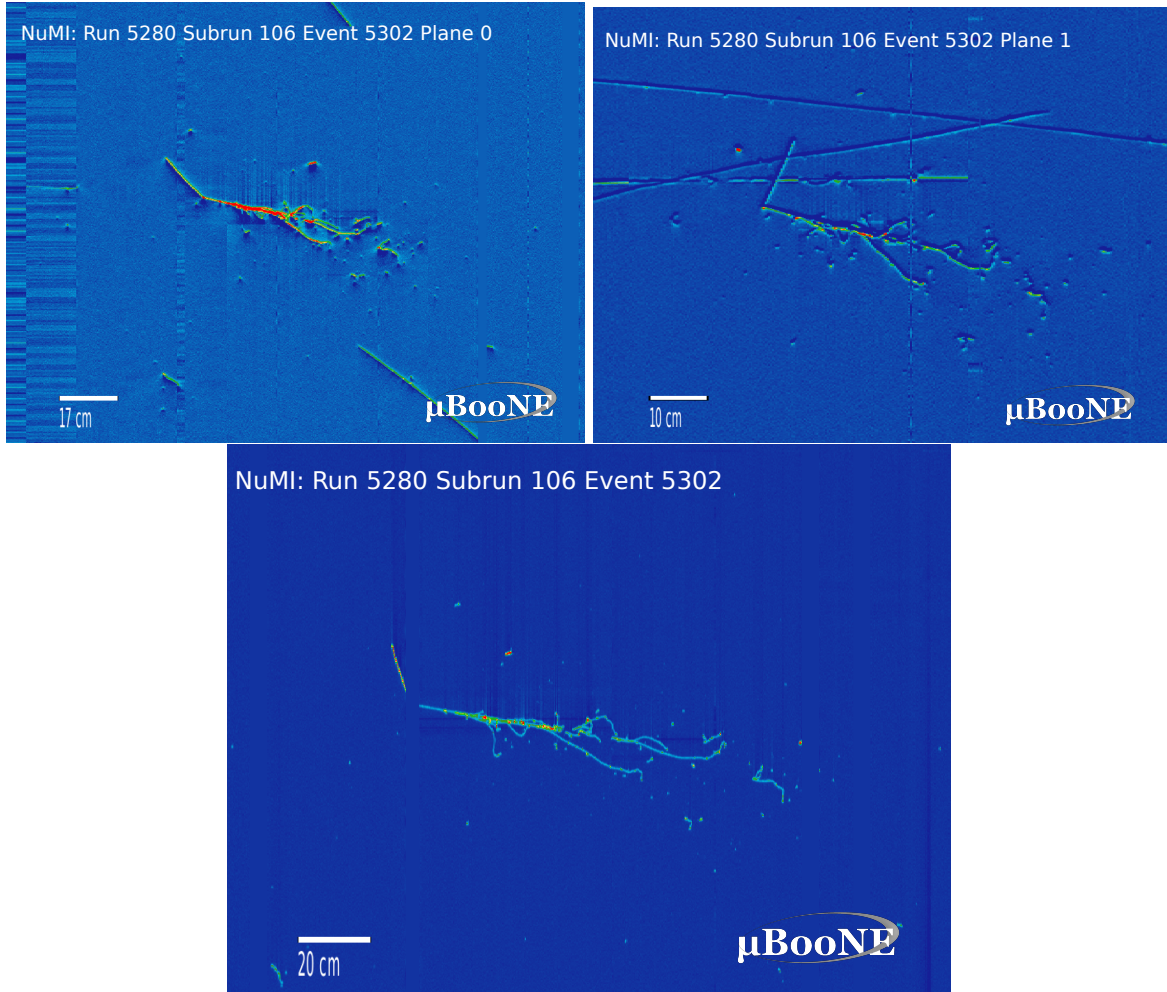


Figure 15: (Top Left) Single shower and single track event reconstructed on the first induction plane. (Top Right) The same event is shown on the second induction plane. The crossing cosmic tracks are not reconstructed with the candidate objects. (Bottom) The same event is now shown on the collection plane. Despite unresponsive wires near the interaction vertex, the ability to use the other two planes keeps the reconstruction precise.

The event displays 16, 17 and 18 show a wider variety of final-state topologies found to pass the inclusive selection. Figure 16 has a more complex topology with three clearly independent tracks originating from the candidate neutrino interaction vertex, as well as a complex shower topology. Near to the interaction vertex, the shower object leaves a charge deposition, leading to the assumption that this is an electron-induced shower. There are also some smaller shower objects separated from the primary shower, which may indicate a π^0 decay.

Figure 17 shows a single shower topology, whose shower is travelling in the direction of electron neutrinos originating from the NuMI target. This visualises the ability to select neutrino candidate events without a corresponding reconstructed track.

The primary shower in Figure 18 is also consistent with the direction of the NuMI target. The varied topology here emphasizes the usefulness of the inclusive for studying different candidate neutrino interactions.

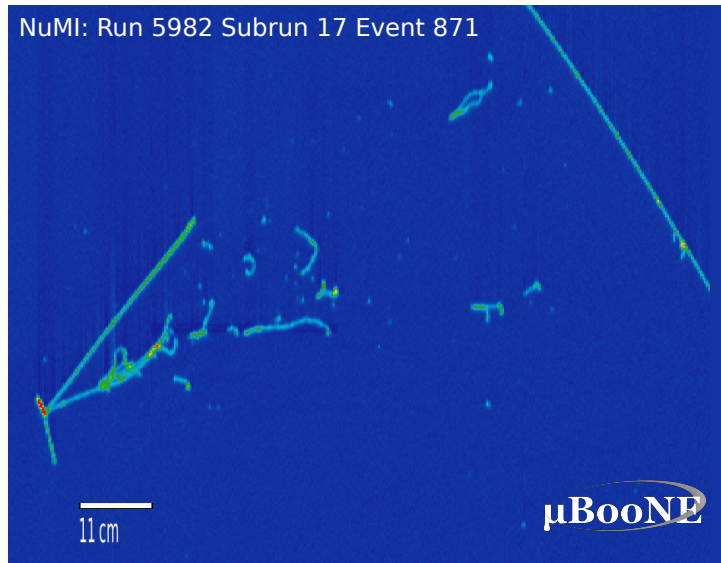


Figure 16: Relatively complex topology that passes the inclusive selection. Several tracks are obviously present, and potentially an electron-induced shower with a π^0 decay.

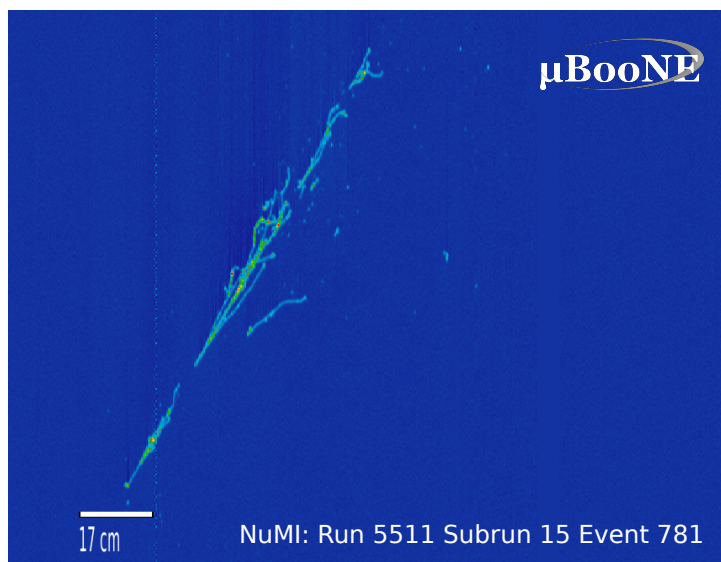


Figure 17: Selected single shower ν_e candidate event. The direction of the shower is consistent with the direction of the NuMI target, from which the majority of neutrinos originate.

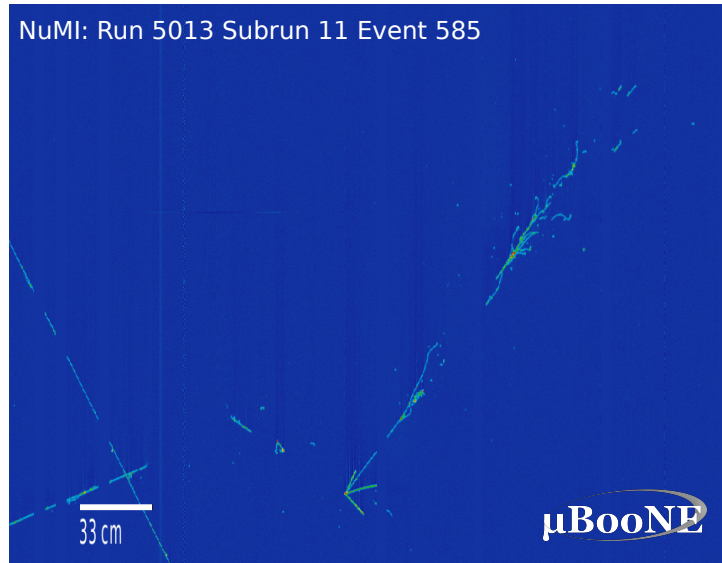


Figure 18: More complex neutrino candidate topology, with several tracks originating from the candidate vertex.

References

- [1] R. Acciarri et al. “Design and Construction of the MicroBooNE Detector”. In: *JINST* 12.02 (2017), P02017. DOI: 10.1088/1748-0221/12/02/P02017. arXiv: 1612.05824 [physics.ins-det].
- [2] R. Acciarri *et al.* “A Proposal for a Three Detector Short-Baseline Neutrino Oscillation Program in the Fermilab Booster Neutrino Beam”. In: (2015).
- [3] LBNE Collaboration. “The Long-Baseline Neutrino Experiment: Exploring Fundamental Symmetries of the Universe”. In: (2014).
- [4] Minerva Collaboration. “Measurement of electron neutrino quasielastic and quasielastic-like scattering on hydrocarbon at $E_\nu = 3.6$ GeV”. In: (2016).
- [5] T2K Collaboration. “Measurement of the Inclusive Electron Neutrino Charged Current Cross Section on Carbon with the T2K Near Detector”. In: (2014).
- [6] MicroBooNE Collaboration. “The Pandora multi-algorithm approach to automated pattern recognition in LAr TPC detectors”. In: (2016).
- [7] P. Adamson *et al.* “The NuMI Neutrino Beam”. In: (2015).
- [8] MiniBooNE Collaboration. “First Measurement of ν_μ and ν_e Events in an Off-Axis Horn-Focused Neutrino Beam”. In: (2009).
- [9] C. Adams et al. “Ionization electron signal processing in single phase LArTPCs. Part II. Data/simulation comparison and performance in MicroBooNE”. In: *JINST* 13.07 (2018), P07007. DOI: 10.1088/1748-0221/13/07/P07007. arXiv: 1804.02583 [physics.ins-det].
- [10] Marco Del Tutto. “NuMu CC Inclusive Analysis”. In: (2018).
- [11] *et al.* Costas Andreopoulos. “The GENIE Neutrino Monte Carlo Generator: Physics and User Manual”. In: (2015).
- [12] The MicroBooNE Collaboration. “Cosmic Shielding Studies at MicroBooNE”. In: (2016).
- [13] ArgoNeuT Collaboration. “First Observation of Low Energy Electron Neutrinos in a Liquid Argon Time Projection Chamber”. In: (2017).